Article

MXene-Based Fiber-Optic Humidity Sensor for Fast Human Breath Monitoring

Xiaokang Li [1], Binchuan Sun [1], Ting Xue [1], Kangwei Pan [1], Yuhui Su [1], Yajun Jiang [1], Bobo Du [2,*] and Dexing Yang [1,*]

1   Shaanxi Key Laboratory of Optical Information Technology, and Key Laboratory of Light-Field Manipulation and Information Acquisition, Ministry of Industry and Information Technology, School of Physical Science and Technology, Northwestern Polytechnical University, Xi'an 710129, China
2   Key Laboratory of Physical Electronics and Devices of Ministry of Education, School of Electronic Science and Engineering, Xi'an Jiaotong University, Xi'an 710049, China
*   Correspondence: bobo.du@xjtu.edu.cn (B.D.); dxyang@nwpu.edu.cn (D.Y.)

Abstract: Breath is one of the most important physiological features of human life. In particular, it is significant to monitor the physical characteristics of breath, such as breath frequency and tidal volume. Breath sensors play an important role in the field of human health monitoring. However, an electronic breath sensor is not stable or even safe when the patient is in a Magnetic Resonance Imaging (MRI) system or during any oncology treatment that requires radiation and other high electric/magnetic fields. Fiber-optic-based sensors have attracted a considerable amount of attention from researchers since they are immune to electromagnetic interference. Here, we propose and demonstrate a fiber-optic-based relative-humidity (RH)-sensing strategy by depositing $Ti_3C_2T_x$ nanosheets onto an etched single-mode fiber (ESMF). The humidity sensor function is realized by modulating the transmitted light in the ESMF using the excellent hydrophilic properties of $Ti_3C_2T_x$. Experiments show that the coated $Ti_3C_2T_x$ nanosheets can effectively modulate the transmitted light in the ESMF in the relative humidity range of 30~80% RH. The sensor's fast response time of 0.176 s and recovery time of 0.521 s allow it to be suitable for real-time human breath monitoring. The effective recognition of different breath rhythms, including fast, normal, deep, and strong breathing patterns, has been realized. This work demonstrates an all-optical $Ti_3C_2T_x$-based sensing platform that combines $Ti_3C_2T_x$ with an optical fiber for humidity sensing for the first time, which has great promise for breath monitoring and presents novel options for gas-monitoring applications in the biomedical and chemical fields.

Keywords: MXene; fiber-optic; humidity sensor; human breath

1. Introduction

Relative humidity (RH) measurements are important for electronic products, industrial and agricultural production, human comfort and health, and precision instrument manufacturing [1–3]. Therefore, the research and development of humidity sensors with excellent sensing characteristics and easy fabrication is significant. Electronic humidity sensors with different operating mechanisms, such as capacitive [4], resistive [5], and field-effect transistors [6], have been developed. High-performance humidity sensors require high sensitivity, excellent survivability, a wide dynamic range, and fast response and recovery times [7]. However, traditional electronic RH sensors have many drawbacks in practical applications, such as their bulky size, complex operation, and poor survivability in electromagnetic interference environments [8]. Fiber-optic humidity sensors have advantages such as a compact structure, anti-electromagnetic interference, a fast response, and the ability to measure remotely, in contrast to traditional sensors [9–11]. Many RH-sensing techniques based on fiber-optic structures, such as fiber Bragg gratings, tilted fiber gratings, fiber facets, interference structures, side-polished fibers, and microfibers, have been reported [12–17]. Actually, these fiber structures are inherently sensitive only to physical parameters (i.e., temperature and strain).

For the purpose of humidity sensing, coatings of hygroscopic materials are always required on the surfaces of these fiber devices. For example, the surface of the FBG must be coated with a material (e.g., polyimide) that has hygroscopic expansion properties since the FBG has only a core mode. The variations in humidity are sensed by applying strain to the FBG through the hygroscopic expansion of the material [12]. Unfortunately, these polymer-based hygroscopic materials have a relatively slow humidity response and considerable hysteresis. Fast-response and high-robustness humidity sensing can be achieved by coating materials that have a refractive index sensitive to moisture onto the surface of the device, e.g., optical fibers with an evanescent field or cladding mode [16,17]. In addition to the advantages of standard optical fibers, microfibers are expected to achieve higher sensitivity compared to other fiber structures since they have a strong evanescent field outside the fiber surface, which can penetrate the coating and enhance light–matter interactions [18]. In order to achieve high sensitivity for RH detection, it is also necessary to add hygroscopic materials to the bare microfiber structure [19]. Therefore, the parameters, such as intensity and wavelength, of the optical signal transmitted in the microfiber will be modulated by the coating of the surface hygroscopic material when the RH in the environment changes. The RH variations can be obtained by demodulating parameters such as the optical intensity and wavelength. [20].

Transition-metal carbides, nitrides, and carbonitrides (normally referred to as MXenes) have been the most attractive family of 2D materials in recent years. The general formula is $M_{n+1}X_nT_x$ ($n = 1$, 2, or 3), where M is an early-transition-metal element (Sc, Ti, etc.), X is C and/or N, and T is the surface termination inherited by the synthesis process, usually $-OH$, $-O$, or $-F$ [21]. There are more than 30 different experimental stoichiometric MXenes and more than 100 (not considering surface termination) theoretically predicted MXenes. MXenes have significant physical and chemical properties, including hydrophilicity, excellent electrical conductivity, a large specific surface area, modifiable functional groups, and favorable biocompatibility [22–24]. These unique properties exhibited by 2D MXene materials possess significant opportunities for many applications, such as electromagnetic shielding [25], photothermal therapy [26], all-optical modulation [27], and sensing [28,29]. In recent years, $Ti_{n+1}C_nT_x$ ($n = 1,2,3$) MXenes have become ideal sensing materials due to their large specific surface area, excellent mechanical stability, outstanding electrical conductivity, and good hydrophilicity [30]. $Ti_3C_2T_x$ is one of the most representative MXenes, consisting of two layers of carbon atoms sandwiched between three layers of titanium atoms to form a sandwich structure. It represents the rise of MXenes, as it is not only the earliest MXene material discovered and successfully fabricated but also the most widely studied among the MXene family, including its preparation methods, physical properties, and application fields [31]. Owing to the advantages of high stability and a relatively simple synthesis method, $Ti_3C_2T_x$ MXene has become the focus of many research efforts [32]. $Ti_3C_2T_x$ MXene has been used in gas sensing [33–37]. It has been shown that the $Ti_3C_2T_x$ sensor has the capacity to measure ethanol, methanol, acetone, and ammonia gases at room temperature and displays p-type sensing behavior. The theoretically calculated detection limit for acetone gas is about 9.27 ppm with this sensor, which has a better performance compared to other 2D-material-based sensors [33]. Multilayered $Ti_3C_2T_x$ sheets have hydrophilic active sites for water adsorption and intercalation due to the presence of -OH-, -O-, and -F-terminated groups [34]. Thus, these properties enable $Ti_3C_2T_x$ to be used as a hygroscopic material for RH sensing. Recently, $Ti_3C_2T_x$ has been applied to RH sensors using electronic methods [35–37]. However, reports of fiber-optic humidity sensors based on $Ti_3C_2T_x$ are relatively few.

In this work, we deposited $Ti_3C_2T_x$ nanosheets onto an etched single-mode fiber (ESMF) for the first time, utilizing the unique properties of $Ti_3C_2T_x$ to realize a high-performance relative humidity (RH) sensor for human breath monitoring. Our work will not only facilitate the achievement of $Ti_3C_2T_x$ in real applications but also emphasize the potential of $Ti_3C_2T_x$ in fiber-optic communities. Owing to the large surface-specific area and abundant hydrophilic functional groups of $Ti_3C_2T_x$ nanosheets, the water molecules can be maximally absorbed, which leads to a change in the refractive index (RI) and the

expansion of the interlayer spacing of the $Ti_3C_2T_x$ thin film [38]. Therefore, the modulation of the ESMF output optical power by the ambient RH is realized. The humidity detection capability of the sensor was tested experimentally with breath patterns, and the results show that the $Ti_3C_2T_x$-based fiber-optic sensor has a fast humidity response speed and exhibits excellent breath-monitoring performance. Moreover, the humidity sensor can be used for the real-time monitoring of human breath with different rhythms. Compared with other fiber-optic structures, the ESMF has the advantages of a simple structure, a strong evanescent field, a low demand for optic devices, and cost-effectiveness. In addition, due to the fast response time of the sensor, RH can be monitored in real time by detecting the intensity of the optical transmission signal. It has potential applications in industrial and agricultural production and human health monitoring.

2. Experiments

In this study, we successfully developed a humidity sensor using $Ti_3C_2T_x$ nanosheets integrated with an etched single-mode fiber (ESMF). The ESMF was obtained from a single-mode fiber (SMF-28), which has a diameter of 125μm and a fiber core diameter of ~9 μm, using the process of chemical etching with hydrofluoric acid. In order to enhance the mechanical stability of the sensor and to facilitate subsequent experiments, the prepared ESMF was fixed to a glass slide and then rinsed three times with deionized water (DI) and ethanol. To improve the RH sensitivity of the ESMF, it is necessary to modify its surface by depositing a $Ti_3C_2T_x$ layer with abundant hydrophilic groups. $Ti_3C_2T_x$ nanosheets were deposited on the sidewalls of the ESMF via natural evaporation, as described in our previous work [27], and aided by optical adsorption. The method of natural evaporation has the advantages of low cost and high efficiency, and the operation process is as follows: Firstly, a $Ti_3C_2T_x$ aqueous suspension with a concentration (XFK08, XFNANO) of 2 mg/mL is dropped onto the ESMF. The $Ti_3C_2T_x$-coated ESMF (TESMF) is then allowed to evaporate naturally for 6 h. Meanwhile, $Ti_3C_2T_x$ nanosheets are attached to the surface of the ESMF using the optical tweezer effect. $Ti_3C_2T_x$ nanosheets could be easily attached to the fiber surface by connecting a 980 nm light source (100 mW) to one end of the ESMF, which effectively accelerates the deposition process. Then, the final $Ti_3C_2T_x$-coated ESMF humidity sensor is fabricated. The 2D morphological characteristics of $Ti_3C_2T_x$ were observed using field-emission scanning electron microscopy (SEM; FEI Verios G4, Waltham, MA, USA) and transmission electron microscopy (TEM; FEI Talos F200X, Waltham, MA, USA), as shown in Figures 1a and 1b, respectively, which also demonstrate the dimension distribution. The structural characteristics of $Ti_3C_2T_x$, as seen in Figure 1a,b, indicate a 2D ultrathin-layer configuration and a morphology resembling a sheet. Figure 1c shows an optical micrograph of the ESMF after it was coated with $Ti_3C_2T_x$. The optical image of the ESMF prior to coating can be seen in the inset. The effective coating of $Ti_3C_2T_x$ nanosheets onto the ESMF surface is evident. In addition, it can be noticed that although the $Ti_3C_2T_x$ nanosheets are successfully coated on the ESMF surface, the coating on the ESMF is relatively rough, which may be caused by the roughness of the ESMF surface after HF etching. This could be further improved by using a finer and more uniform dispersion. The surface roughness of the ESMF may be one of the influential factors in the larger response of the sensor in the high-humidity range. Figure 1d shows the coating morphology tested by scanning electron microscopy (SEM). The $Ti_3C_2T_x$ coating exhibits sharp edges. This is an attractive feature of the sensor that may contribute to the enhanced humidity and gas response, which is utilized in our work.
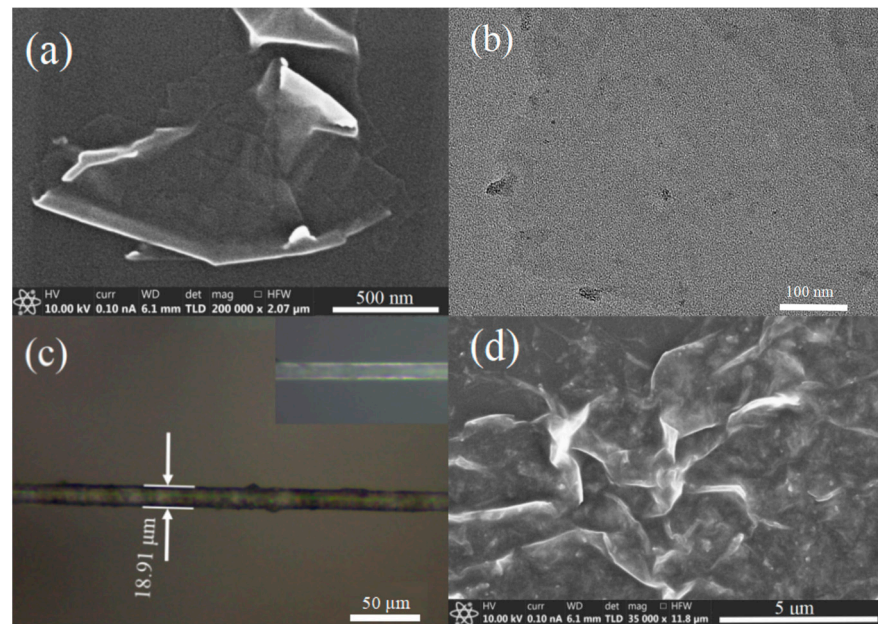
Figure 1. (**a**) SEM image of the $Ti_3C_2T_x$ nanosheet; (**b**) TEM image of the $Ti_3C_2T_x$ nanosheet; (**c**) optical microscope image of the TESMF (the inset in (**c**) is uncoated ESMF); (**d**) SEM image of the TESMF.

To evaluate the RH response of the TESMF, an experimental setup was designed by our team, as shown in Figure 2. The experimental setup includes a Yokogawa AQ2211 Frame Controller, which serves as a stable laser source; an EXCAL 1421-HE environmental test chamber with program-controlled temperature and humidity settings; and a Yokogawa AQ2200-221 Sensor Module acting as a photo-detector. A laser with a wavelength of 1540 nm is launched into the TESMF, and the photo-detector measures the transmitted light power. The schematic structure of the proposed $Ti_3C_2T_x$-nanosheet-coated ESMF is shown in Figure 2. The two side regions of the TESMF remain a standard SMF, and the middle region, which is thinned by etching, is coated with $Ti_3C_2T_x$ nanosheets on the surface to enhance the moisture sensitivity. When the incident light is transmitted to the TESMF, the incident light initially interacts with the $Ti_3C_2T_x$ film in the ESMF region covered by the $Ti_3C_2T_x$ nanosheets due to the strong evanescent waves of the ESMF. The hydrophilic functional groups located on the surface of $Ti_3C_2T_x$ have the ability to selectively retain or release water molecules through the formation of hydrogen bonds. This characteristic enables the material to efficiently interact with water molecules nearby. The transmitted optical power will rise with increasing ambient RH, which should be the result of the decreasing absorption of the evanescent field by the $Ti_3C_2T_x$ film. After absorbing a specific number of water molecules, the $Ti_3C_2T_x$ film exhibits alterations in its surface characteristics, resulting in the expansion of the interlayer gap [23]. As a result, the loss of the $Ti_3C_2T_x$ film to the incident light is changed, ultimately affecting the output optical signal. Therefore, the level of transmitted power depends on the variation in RH. A highly sensitive humidity sensor can be developed by monitoring the transmitted power of the TESMF.

In the experiment, the ESMF was placed in a humidity environmental chamber for humidity-sensing tests. A commercially integrated humidity/temperature meter was employed to observe and record the standard levels of humidity and temperature. During the RH-sensing tests, the temperature within the environmental chamber was adjusted to 40 °C, while the RH was systematically varied in a cyclical manner. The RH was gradually raised from 30% to 80% in 10% intervals, with the adjustments being made automatically. Each humidity level was maintained for a duration of 30 min in order to achieve stabilization. Subsequently, the humidity level was reduced from 80% to 30%

while maintaining a consistent interval of humidity change. The transmitted light power and RH were recorded during the whole experimental process. To accomplish human breath measurements, the sensor, with RH testing completed, was removed from the environmental chamber. Subsequently, breath tests were directed toward the sensor for analysis. Meanwhile, the power of the transmitted light was monitored.
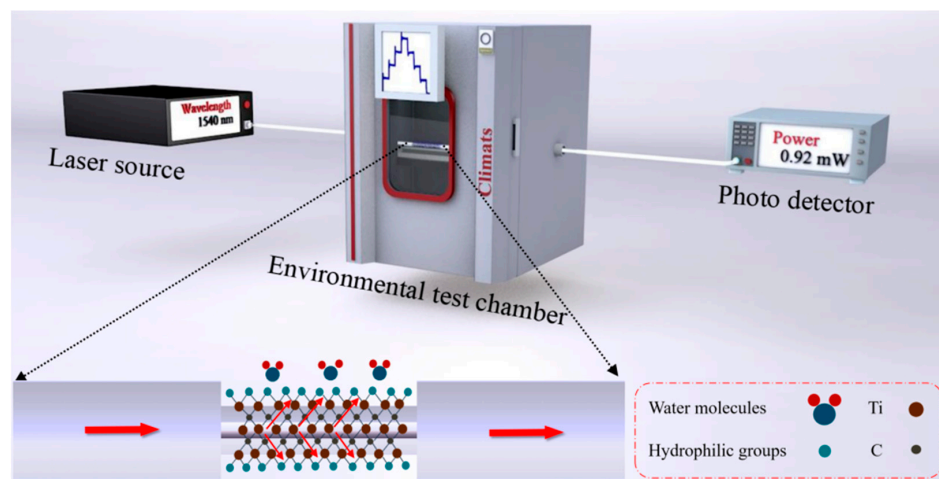

Figure 2. Experimental setup for RH measurement with the sensor. The inset is the working principle of the sensor.

3. Results and Discussion

In order to evaluate the detecting properties of the RH sensor, it was positioned within an environmental test chamber. The RH level within the chamber was then raised and subsequently decreased. The curve of RH with time set by the temperature and humidity test chamber consists of a group of symmetrical standard step-like curves. The temperature during the experiment was set to 40 °C. The whole experimental cycle was 6 h in total, and the first three hours of the RH curve increase is defined as the RH rising process, and accordingly, the last three hours of the RH curve decrease is defined as the RH falling process. Figure 3a illustrates the dependence of RH on time, as determined by the sensor integrated into the test chamber. The presence of spike-like fluctuations in the humidity curve during the beginning stage of each new humidity step in the experiment can be attributed to the feedback regulation between the RH and temperature within the test chamber. Figure 3b depicts the observed variation curve of transmitted light power in relation to humidity, as measured by the sensor that was developed in the present work. The experimental cycle exhibits a significant influence on the transmitted power of the sensor, as it is seen that the power is closely linked to the real fluctuations in RH. This is verified by the occurrence of step characteristics and peak-like fluctuations in the optical power curve corresponding to the RH curve.

The humidity sensor function is realized by modulating the transmitted light of the ESMF using the excellent hydrophilic properties of $Ti_3C_2T_x$. The optical power of the ESMF transmission can be modulated by absorbing and incorporating the surrounding water molecules into the $Ti_3C_2T_x$ film. Humidity variations will lead to changes in the transmitted power of the ESMF. This is attributed to the modulation of the swift field by the $Ti_3C_2T_x$ film. The sensing characteristics of the sensor were measured using ascending and descending methods over a relative humidity level range of 30% ~ 80%. The response of the $Ti_3C_2T_x$-deposited ESMF to humidity is reversible due to the absorption and desorption of water molecules by $Ti_3C_2T_x$. The data points depicted in Figure 4 illustrate the average transmitted power at 30 min intervals. Specifically, the square data points reflect the average power during the rising stage of RH, while the circular data points relate to the average power during the dropping process. It can be seen that as RH increases from 30% to 80%, the transmitted power increases non-linearly from 1.608 mW to 1.64 mW for each

10% increase. Conversely, when RH decreases from 80% to 30%, the transmitted power decreases non-linearly from 1.64 mW to 1.611 mW for each 10% decrease. The results show that the power of the output optical signal can change with ambient RH. In order to improve the long-term stability of the fiber-based humidity sensor in practical applications, an effective package is also needed, which will be studied in our follow-up work. The variation in the transmitted power is more significant in the high-humidity range. This is due to the fact that the surface coating of the $Ti_3C_2T_x$-integrated ESMF device has a certain roughness, and when the $Ti_3C_2T_x$ coating absorbs a certain number of water molecules, the interlayer spacing between the layers of the $Ti_3C_2T_x$ film is widened. This results in a more uniform thickness of the $Ti_3C_2T_x$ film in the sensing region, which further reduces the loss of transmitted light. Similarly, the fabricated sensor has the potential for application in breath sensing due to the fact that breath can cause a change in RH in the environment.
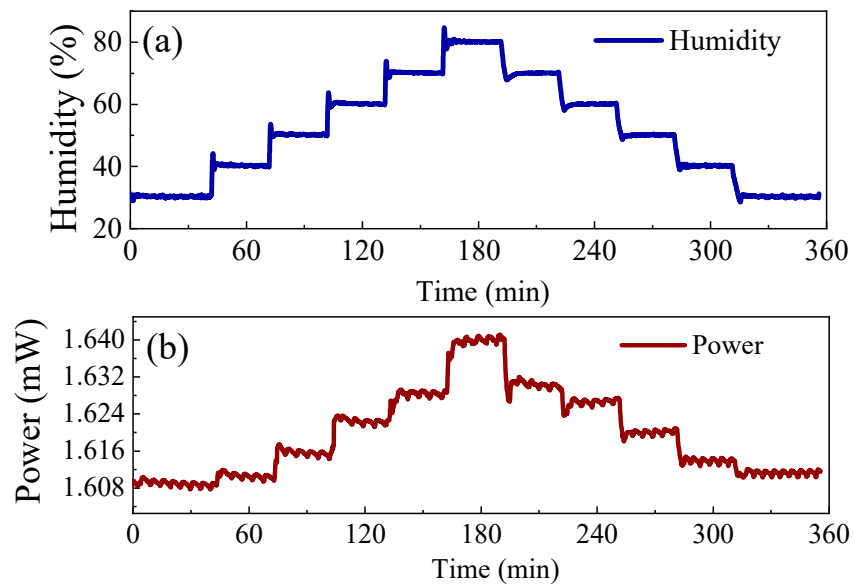

Figure 3. (**a**) RH in the chamber measured by a capacitance hygrometer integrated within the environmental test chamber; (**b**) the variation in the transmitted optical power in the sensor.
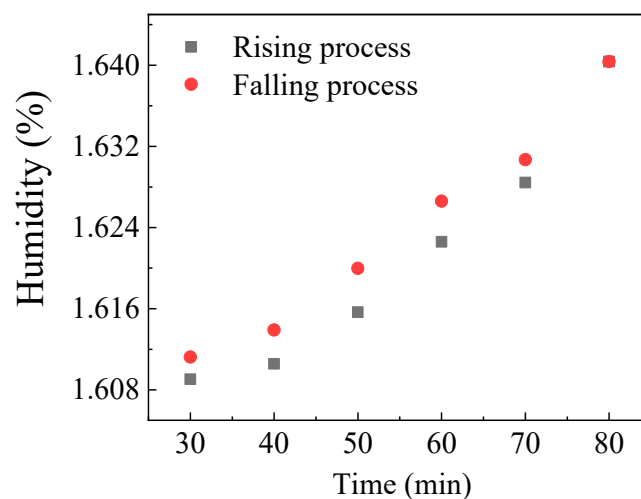
Figure 4. The time average of transmitted power with different RH levels.

An interesting research objective is the application of an all-fiber-optic humidity sensor based on $Ti_3C_2T_x$ to human breath monitoring. To obtain breath response characteristics, we directly monitored human breath with different breathing patterns. The experimental

setup for human breath monitoring is shown in Figure 5a. A laser with a wavelength of 1540 nm is launched into the sensor, and the breath is directed to the sensor. Meanwhile, the transmitted light power is monitored. Since human breath contains a large amount of water vapor and the humidity around the sensor changes locally by around 10%RH [39,40], the transmitted light power of the sensor is similarly modulated by the breathing process. To verify the time-response performance of the sensor, we conducted an exhalation/inhalation cycle test on the sensor. Figure 5b illustrates the periodical fluctuations in transmitted power observed during a single breath cycle. The power of transmitted light varies with the exhale/inhale cycle. The measurements indicate a rapid increase in optical power due to the exposure of the sensor to inhaled moisture and a decrease toward the original power level after reaching a peak. The maximum power change is about 0.02 mW. To analyze the time-response characteristics of the sensor, data from the expiratory/inspiratory phases were fitted using exponential equations $P = P_1 + A_1 \cdot \exp[-(t - t_1)/t_{response}](P = P_2 + A_2 \cdot \exp[-(t - t_2)/t_{recovery}])$, where P, P_1, and P_2 represent the optical power; A_1 and A_2 are the fitting coefficients; and t, t_1, and t_2 are time. A fast breath response was achieved, and the obtained response time ($t_{response}$) and recovery time ($t_{recovery}$) are 0.179 s and 0.521 s, respectively. The corresponding R^2 coefficients are 0.99374 and 0.9966, respectively, indicating the high accuracy of the measurements. To investigate the performance of the sensors in depth, a scheme for directly monitoring the fluctuations in human breath was adopted. The power signal exhibits periodic variations when the breath airflow comes into contact with the sensor, as shown in Figure 5c. Different fluctuations in the breath airflow lead to periodic changes in the power signal with different amplitudes. The sensor exhibits good repeatability and reliability during the breath cycle. The above results indicate that the sensor has a higher frequency resolution than the normal respiratory rate (16-20 breaths per minute) and can be used in practical nursing applications.
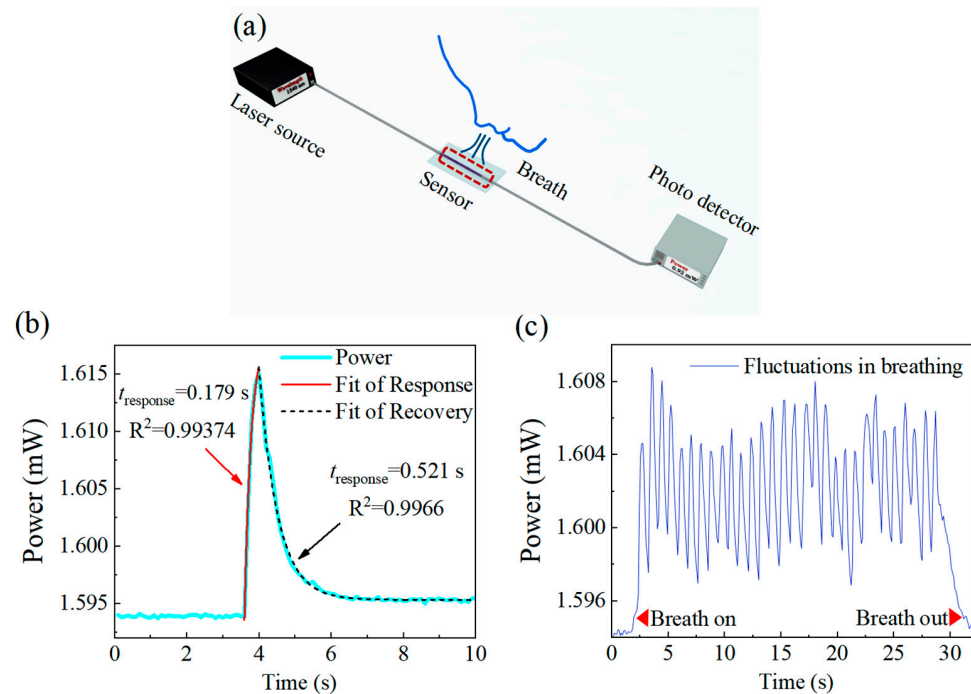
Figure 5. (**a**) Experimental setup for monitoring human breath; (**b**) the response characteristics of the sensor to one single expiration/inspiration cycle; (**c**) the monitoring of human breath fluctuations by the sensor.

In order to further evaluate the response characteristics of the sensor to different breath patterns and breath frequencies, we further designed a verification experiment on the breath-sensing performance of the sensor. As shown in Figure 6, when the breathing

airflow contacts the sensor with different rhythms, including fast, normal, deep, and strong breathing, the transmitted light power of the sensor changes periodically, indicating that the sensor has good repeatability and reliability during the breathing cycle. The results of the verification experiments show that the sensor can recognize different patterns of breath. The sensor has an excellent response to different breath characteristics and offers reliable stability. It can be used to monitor breath patterns for patients with different health conditions. Hence, it has potential applications in the field of practical human health monitoring.
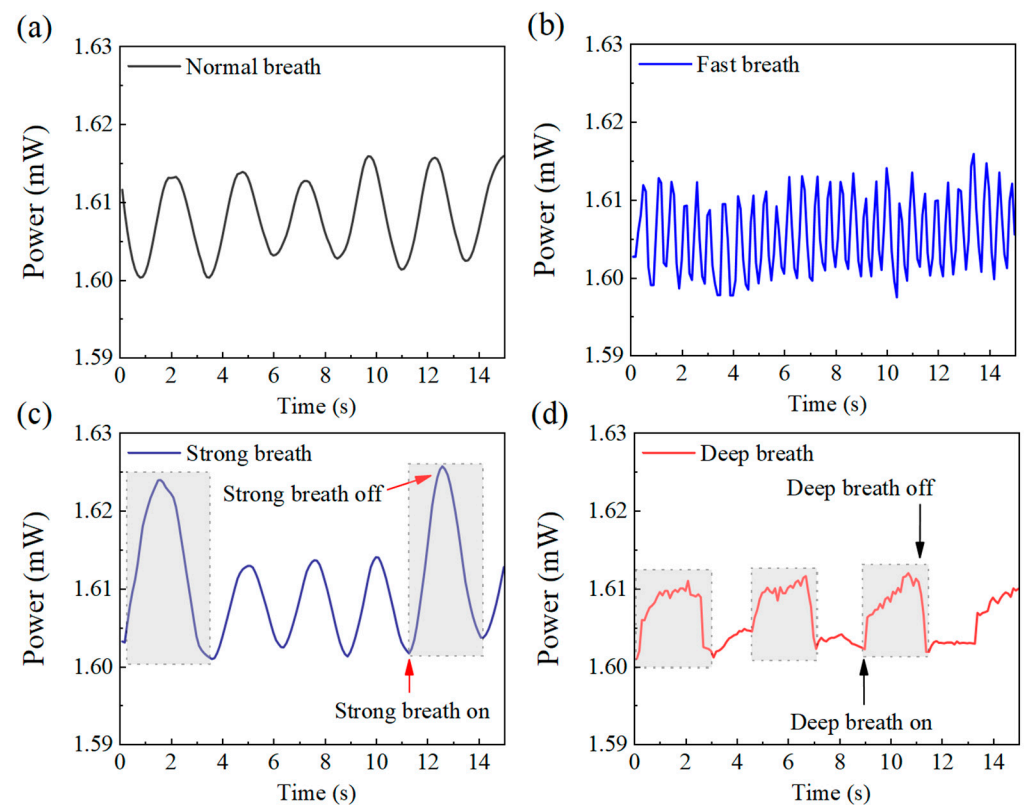
Figure 6. Response of the proposed sensor to different breath patterns, including (**a**) normal breath, (**b**) fast breathing, (**c**) strong breath, and (**d**) deep breath.

Fiber optics provide an ideal platform for photonic integrated devices for 2D materials. In particular, fiber-based sensors are resistant to electromagnetic interference and have anti-corrosion properties, a fast response, and remote measurement capabilities. Table 1 presents a comparative analysis of the performance of humidity sensors employing different fiber-optic designs. The results show that the proposed $Ti_3C_2T_x$-coated micro-nano-fiber-optic humidity sensor has a fast-response performance. This is due to the presence of $-OH$, $-O$, and $-F$ terminal groups in the multilayered $Ti_3C_2T_x$ sheets that provide abundant hydrophilic active sites for water adsorption, and $Ti_3C_2T_x$ MXene has the advantage of a high specific surface area. The total time (sum of response time and recovery time) of the $Ti_3C_2T_x$-based sensor is the smallest (0.697 s) compared to other fiber-optic RH sensors. This is essential in practical gas monitoring and human health monitoring. Furthermore, the integration of $Ti_3C_2T_x$ nanosheets with the micro-nano-fiber presents a very attractive scheme for applications in RH sensing. It can also provide guidance for the future development of fast-response gas sensors. However, pristine MXenes have poor selectivity for water, as $Ti_3C_2T_x$ proved to be very sensitive to rather low concentrations of ketones (<50 ppb) [33,41], alcohols (<100 ppb) [42], and ammonia (<100 ppb) [43] vapors at room temperature. The practical performance of MXene-based humidity sensors on gas selectivity still needs to be improved [44]. It is possible to further functionalize the $Ti_3C_2T_x$ surfaces to realize a $Ti_3C_2T_x$-integrated fiber sensor with gas-selective capability.

Table 1. Performance comparison of RH sensors based on different fiber-optic structures.

Structure	Material	Response Time/s	Recovery Time/s	Reference
Microfiber	g-CN	0.43	0.87	[20]
Microfiber interferometer	Nb2CTX	1.76	5.71	[29]
Side-polished fiber	WS2	1	5	[45]
Hollow-core fiber	RGO	5.2	8.1	[46]
ESMF	Ti3C2Tx	0.176	0.521	This work

4. Conclusions

In conclusion, we proposed and investigated a fiber-optic humidity sensor based on $Ti_3C_2T_x$-integrated microfibers. $Ti_3C_2T_x$ nanosheets are deposited on the ESMF surface via the photo-deposition method, and the sensor is used for RH measurement. Investigations based on optical microscopy, SEM, and TEM verify effective and tight $Ti_3C_2T_x$ deposition. Since water adsorption changes the layer spacing of the $Ti_3C_2T_x$ film and $Ti_3C_2T_x$ has a large specific surface area, the evanescent waves in the ESMF are significantly modulated by changes in RH and ultimately lead to a corresponding change in the transmitted optical power. The distinctive humidity mechanism is demonstrated at different levels of RH, and the sensor exhibits a non-linear response to variations in RH. The effects of the thickness of the $Ti_3C_2T_x$ film and the diameter of the ESMF on the non-linear response mechanism and sensing sensitivity will be investigated in our subsequent work. Furthermore, the sensor has excellent performance in detecting variations in human breath, with fast response and recovery times of 0.176 s and 0.521 s, respectively. It also enabled the monitoring of human breath with different rhythms. Thus, this RH sensor, characterized by repeatability and a fast response, is a promising alternative for settings requiring compact equipment and the detection of dynamic changes in RH, such as industrial and agricultural production, meteorology, and human health monitoring.

Author Contributions: Conceptualization, X.L. and D.Y.; validation, X.L., B.S. and T.X.; investigation, K.P.; data curation, Y.S. and Y.J.; writing—original draft preparation, X.L.; writing—review and editing, B.D.; visualization, T.X.; supervision, D.Y. All authors have read and agreed to the published version of the manuscript.

Institutional Review Board Statement: Not applicable.

Informed Consent Statement: Informed consent was obtained from all subjects involved in the study.

Data Availability Statement: The data presented in this study are available on request from the corresponding author.

Conflicts of Interest: The authors declare no conflict of interest.

References

1. Duan, Z.; Jiang, Y.; Tai, H. Recent advances in humidity sensors for human body related humidity detection. *J. Mater. Chem. C* **2021**, *9*, 14963–14980. [CrossRef]
2. Mihailov, S.J.; Ding, H.; Hnatovsky, C.; Walker, R.B.; Lu, P.; De Silva, M. Through-The-Coating Fabrication of Fiber Bragg Grating Relative Humidity Sensors Using Femtosecond Pulse Duration Infrared Lasers and a Phase Mask. *Photonics* **2023**, *10*, 625. [CrossRef]
3. Guan, X.; Hou, Z.; Wu, K.; Zhao, H.; Liu, S.; Fei, T.; Zhang, T. Flexible humidity sensor based on modified cellulose paper. *Sens. Actuators B Chem.* **2021**, *339*, 129879. [CrossRef]
4. Romero, F.J.; Rivadeneyra, A.; Salinas-Castillo, A.; Ohata, A.; Morales, D.P.; Becherer, M.; Rodriguez, N. Design, fabrication and characterization of capacitive humidity sensors based on emerging flexible technologies. *Sens. Actuators B Chem.* **2019**, *287*, 459–467. [CrossRef]
5. Awais, M.; Khan, M.U.; Hassan, A.; Bae, J.; Chattha, T.E. Printable highly stable and superfast humidity sensor based on two dimensional molybdenum diselenide. *Sci. Rep.* **2020**, *10*, 5509. [CrossRef] [PubMed]
6. Lee, S.P.; Park, K.-J. Humidity sensitive field effect transistors. *Sens. Actuators B Chem.* **1996**, *35*, 80–84. [CrossRef]

7. Waheed, W.; Anwer, S.; Khan, M.U.; Sajjad, M.; Alazzam, A. 2D Ti$_3$C$_2$T$_x$-MXene nanosheets and graphene oxide based highly sensitive humidity sensor for wearable and flexible electronics. *Chem. Eng. J.* **2023**, *480*, 147981. [CrossRef]

8. Wu, X.; Gao, F.; Jin, F.; Wang, D.; Wang, W.; Chen, Q.; Yang, H.; Gong, H.; Wang, Z.; Zhao, C.; et al. Optical fiber humidity sensor with C60-THAM as molecule receptors. *Sens. Actuators B: Chem.* **2022**, *370*, 132344. [CrossRef]

9. Chiu, Y.-D.; Wu, C.-W.; Chiang, C.-C. Tilted fiber Bragg grating sensor with graphene oxide coating for humidity sensing. *Sensors* **2017**, *17*, 2129. [CrossRef]

10. Wang, N.; Tian, W.; Zhang, H.; Yu, X.; Yin, X.; Du, Y.; Li, D. An easily fabricated high performance Fabry-Perot optical fiber humidity sensor filled with graphene quantum dots. *Sensors* **2021**, *21*, 806. [CrossRef]

11. Presti, D.L.; Massaroni, C.; Schena, E. Optical fiber gratings for humidity measurements: A review. *IEEE Sens. J.* **2018**, *18*, 9065–9074. [CrossRef]

12. Wang, W.; Sun, T.; Peng, J.; Dai, J.; Yang, M. Humidity sensor based on fiber Bragg grating coated with different pore-foaming agent doped polyimides. *IEEE Photon-Technol. Lett.* **2017**, *29*, 1963–1966. [CrossRef]

13. Du, B.; Yang, D.; She, X.; Yuan, Y.; Mao, D.; Jiang, Y.; Lu, F. MoS2-based all-fiber humidity sensor for monitoring human breath with fast response and recovery. *Sens. Actuators B Chem.* **2017**, *251*, 180–184. [CrossRef]

14. Lang, C.; Liu, Y.; Cao, K.; Li, Y.; Qu, S. Ultra-compact, fast-responsive and highly-sensitive humidity sensor based on a polymer micro-rod on the end-face of fiber core. *Sens. Actuators B Chem.* **2019**, *290*, 23–27. [CrossRef]

15. Yi, Y.; Jiang, Y.; Zhao, H.; Brambilla, G.; Fan, Y.; Wang, P. High-performance ultrafast humidity sensor based on microknot resonator-assisted Mach–Zehnder for monitoring human breath. *ACS Sens.* **2020**, *5*, 3404–3410. [CrossRef] [PubMed]

16. Li, D.; Lu, H.; Qiu, W.; Dong, J.; Guan, H.; Zhu, W.; Yu, J.; Luo, Y.; Zhang, J.; Chen, Z. Molybdenum disulfide nanosheets deposited on polished optical fiber for humidity sensing and human breath monitoring. *Optics Express* **2017**, *25*, 28407–28416. [CrossRef]

17. Jiang, B.; Bi, Z.; Hao, Z.; Yuan, Q.; Feng, D.; Zhou, K.; Zhang, L.; Gan, X.; Zhao, J. Graphene oxide-deposited tilted fiber grating for ultrafast humidity sensing and human breath monitoring. *Sens. Actuators B Chem.* **2019**, *293*, 336–341. [CrossRef]

18. Lou, J.; Wang, Y.; Tong, L. Microfiber optical sensors: A review. *Sensors* **2014**, *14*, 5823–5844. [CrossRef]

19. Peng, Y.; Zhao, Y.; Chen, M.; Xia, F. Research advances in microfiber humidity sensors. *Small* **2018**, *14*, e1800524. [CrossRef]

20. Yan, Z.; Wang, C.; Yu, R.; Hu, Z.; Xiao, L. Graphitic carbon nitride for enhancing humidity sensing of microfibers. *J. Light. Technol.* **2021**, *39*, 3896–3902. [CrossRef]

21. Naguib, M.; Mochalin, V.N.; Barsoum, M.W.; Gogotsi, Y. Two-dimensional materials: 25th anniversary article: MXenes: A new family of two-dimensional materials. *Adv. Mater.* **2014**, *26*, 982. [CrossRef]

22. Vahid Mohammadi, A.; Rosen, J.; Gogotsi, Y. The world of two-dimensional carbides and nitrides (MXenes). *Science* **2021**, *372*, 1581. [CrossRef] [PubMed]

23. Wang, Y.; Xu, Y.; Hu, M.; Ling, H.; Zhu, X. MXenes: Focus on optical and electronic properties and corresponding applications. *Nanophotonics* **2020**, *9*, 1601–1620. [CrossRef]

24. Jiang, X.; Liu, S.; Liang, W.; Luo, S.; He, Z.; Ge, Y.; Wang, H.; Cao, R.; Zhang, F.; Wen, Q.; et al. Broadband nonlinear photonics in few-layer MXene Ti$_3$C$_2$T$_x$ (T = F, O, or OH). *Laser Photonics Rev.* **2018**, *12*, 1700229. [CrossRef]

25. Hantanasirisakul, H.; Gogotsi, Y. Electronic and optical properties of 2D transition metal carbides and nitrides (MXenes). *Adv. Mater.* **2018**, *30*, 1804779. [CrossRef] [PubMed]

26. Huang, Z.; Cui, X.; Li, S.; Wei, J.; Li, P.; Wang, Y.; Lee, C.-S. Two-dimensional MXene-based materials for photothermal therapy. *Nanophotonics* **2020**, *9*, 2233–2249. [CrossRef]

27. Li, X.; Chong, Y.; Wang, J.; Xue, T.; Yan, J.; Feng, D.; Jiang, Y.; Zou, J.; Du, B.; Yang, D. A linear chirp fiber Bragg grating with tunable bandwidth enabled by MXene's photothermal effect. *Appl. Phys. Lett.* **2023**, *123*, 163504. [CrossRef]

28. Ho, D.H.; Choi, Y.Y.; Jo, S.B.; Myoung, J.; Cho, J.H. Sensing with MXenes: Progress and prospects. *Adv. Mater.* **2021**, *33*, 2005846. [CrossRef]

29. Bi, M.; Miao, Y.; Li, W.; Yao, J. Niobium carbide MXene-optics fiber-sensor for high sensitivity humidity detection. *Appl. Phys. Lett.* **2022**, *120*, 021103. [CrossRef]

30. Dillon, A.D.; Ghidiu, M.J.; Krick, A.L.; Griggs, J.; May, S.J.; Gogotsi, Y.; Barsoum, M.W.; Fafarman, A.T. Highly conductive optical quality solution-processed films of 2D titanium carbide. *Adv. Funct. Mater.* **2016**, *26*, 4162–4168. [CrossRef]

31. Wu, L.; Yuan, X.; Tang, Y.; Wageh, S.; Al-Hartomy, O.A.; Al-Sehemi, A.G.; Yang, J.; Xiang, Y.; Zhang, H.; Qin, Y. MXene sensors based on optical and electrical sensing signals: From biological, chemical, and physical sensing to emerging intelligent and bionic devices. *PhotoniX* **2023**, *4*, 15. [CrossRef]

32. Pei, Y.; Zhang, X.; Hui, Z.; Zhou, J.; Huang, X.; Sun, G.; Huang, W. Ti$_3$C$_2$T$_x$ MXene for sensing applications: Recent progress, design principles, and future perspectives. *ACS Nano* **2021**, *15*, 3996–4017. [CrossRef] [PubMed]

33. Lee, E.; Vahid Mohammadi, A.; Prorok, B.C.; Yoon, Y.S.; Beidaghi, M.; Kim, D.-J. Room temperature gas sensing of two-dimensional titanium carbide (MXene). *ACS Appl. Mater. Interfaces* **2017**, *9*, 37184–37190. [CrossRef]

34. Celerier, S.; Hurand, S.; Garnero, C.; Morisset, S.; Benchakar, M.; Habrioux, A.; Chartier, P.; Mauchamp, V.; Findling, N.; Lanson, B.; et al. Hydration of Ti$_3$C$_2$T$_x$ MXene: An interstratification process with major implications on physical properties. *Chem. Mater.* **2019**, *31*, 454–461. [CrossRef]

35. Wu, J.; Lu, P.; Dai, J.; Zheng, C.; Zhang, T.; Yu, W.W.; Zhang, Y. High performance humidity sensing property of Ti$_3$C$_2$T$_x$ MXene-derived Ti$_3$C$_2$T$_x$/K$_2$Ti$_4$O$_9$ composites. *Sens. Actuators B Chem.* **2021**, *326*, 128969. [CrossRef]

36. An, H.; Habib, T.; Shah, S.; Gao, H.; Patel, A.; Echols, L.; Zhao, X.; Radovic, M.; Green, M.J.; Lutkenhaus, J.L. Water sorption in MXene/polyelectrolyte multilayers for ultrafast humidity sensing. *ACS Appl. Nano Mater.* **2019**, *2*, 948–955. [CrossRef]

37. Chen, J.; Qin, W.; Li, K.; Feng, L.; Chen, J.; Qiao, H.; Yang, M.; Tian, Z.; Li, X.; Gu, C.; et al. A high-sensitivity, fast-response and high-stability humidity sensor of curly flake $Ti_3C_2T_x$ MXene prepared by electrolytic intercalation of NaOH solution. *J. Mater.* **2022**, *10*, 22278–22288. [CrossRef]

38. Wang, L.; Tian, M.; Zhang, Y.; Sun, F.; Qi, X.; Liu, Y.; Qu, L. Helical core-sheath elastic yarn-based dual strain/humidity sensors with MXene sensing layer. *J. Mater. Sci.* **2020**, *55*, 6187–6194. [CrossRef]

39. Kano, S.; Kim, K.; Fujii, M. Fast-response and flexible nanocrystal-based humidity sensor for monitoring human respiration and water evaporation on skin. *ACS Sens.* **2017**, *2*, 828–833. [CrossRef]

40. Du, B.; Yang, D.; Ruan, Y.; Jia, P.; Ebendorff-Heidepriem, H. Compact plasmonic fiber tip for sensitive and fast humidity and human breath monitoring. *Opt. Lett.* **2020**, *45*, 985–988. [CrossRef] [PubMed]

41. Yuan, W.; Yang, K.; Peng, H.; Li, F.; Yin, F. A flexible VOCs sensor based on a 3D Mxene framework with a high sensing performance. *J. Mater. Chem. A* **2018**, *6*, 18116–18124. [CrossRef]

42. Koh, H.-J.; Kim, S.J.; Maleski, K.; Cho, S.-Y.; Kim, Y.-J.; Ahn, C.W.; Gogotsi, Y.; Jung, H.-T. Enhanced selectivity of MXene gas sensors through metal ion intercalation: In situ X-ray diffraction study. *ACS Sens.* **2019**, *4*, 1365–1372. [CrossRef] [PubMed]

43. Wu, M.; He, M.; Hu, Q.; Wu, Q.; Sun, G.; Xie, L.; Zhang, Z.; Zhu, Z.; Zhou, A. Ti_3C_2 MXene-based sensors with high selectivity for NH_3 detection at room temperature. *ACS Sens.* **2019**, *4*, 2763–2770. [CrossRef] [PubMed]

44. Janica, I.; Montes-García, V.; Urban, F.; Hashemi, P.; Nia, A.S.; Feng, X.; Samorì, P.; Ciesielski, A. Covalently Functionalized MXenes for Highly Sensitive Humidity Sensors. *Small Methods* **2023**, *7*, e2201651. [CrossRef]

45. Luo, Y.; Chen, C.; Xia, K.; Peng, S.; Guan, H.; Tang, J.; Lu, H.; Yu, J.; Zhang, J.; Xiao, Y.; et al. Tungsten disulfide (WS_2) based all-fiber-optic humidity sensor. *Opt. Express* **2016**, *24*, 8956–8966. [CrossRef]

46. Gao, R.; Lu, D.; Cheng, J.; Jiang, Y.; Jiang, L.; Qi, Z. Humidity sensor based on power leakage at resonance wavelengths of a hollow core fiber coated with reduced graphene oxide. *Sens. Actuators B Chem.* **2016**, *222*, 618–624. [CrossRef]